

Radio Science

RESEARCH ARTICLE

10.1029/2020RS007140

Special Section:

Beacon Satellite Symposium
2019

Key Points:

- We have compared five Rate Of TEC Index (ROTI) methods to evaluate the most suitable one for analyzing the equatorial ionospheric irregularities
- ROTI index maps are a very effective resource for observing and characterizing plasma bubbles in the Brazilian sector
- The irregularities observed in the ROTI index maps are more evident than in the total electron content maps

Correspondence to:

C. S. Carmo,
carolscarmo25@gmail.com










Citation:

Carmo, C. S., Denardini, C. M., Figueiredo, C. A. O. B., Resende, L. C. A., Picanço, G. A. S., Barbosa Neto, P. F., et al. (2021). Evaluation of different methods for calculating the ROTI index over the Brazilian sector. *Radio Science*, 56, e2020RS007140. <https://doi.org/10.1029/2020RS007140>

Received 4 JUN 2020

Accepted 5 JUN 2021

Evaluation of Different Methods for Calculating the ROTI Index Over the Brazilian Sector

C. S. Carmo¹ , C. M. Denardini¹ , C. A. O. B. Figueiredo¹ , L. C. A. Resende^{1,2} ,
G. A. S. Picanço¹ , P. F. Barbosa Neto^{1,3} , P. A. B. Nogueira⁴ , J. Moro^{2,5} , and S. S. Chen¹ 

¹National Institute for Space Research (INPE), São José dos Campos, Brazil, ²State Key Laboratory of Space Weather (NSSC/CAS), Beijing, China, ³Salesian University Center of São Paulo, Lorena, Brazil, ⁴Federal Institute of Education, Science and Technology of São Paulo (IFSP), Jacareí, Brazil, ⁵Southern Space Coordination (COESU/INPE), Santa Maria, Brazil

Abstract Ionospheric irregularities as plasma bubbles occur in the ionosphere, and generally, they are characterized by the low plasma density regions. The Rate Of TEC Index (ROTI) was defined in terms of the Total Electron Content (TEC) variation and is used to characterize these plasma bubbles. It is essential to evaluate the ROTI behavior since the ionospheric irregularities can cause fluctuations in the radio signal, interfering in the ionospheric data analysis. Therefore, we performed in this work a comparative study of five different methods available to calculate the ROTI to evaluate the most suitable over the Brazilian region. The ROTI was calculated over three GNSS stations at different latitudes: São Luís (SALU, 2°31'S, 44°16'W; dip: −3.8°), Cachoeira Paulista (CHPI, 22°40'S, 44°59'W; dip: −36.4°), and Santa Maria (SMAR, 29°41'S, 53°48'W, dip: −37°). The results show that the most viable method for calculating ROTI in the Brazilian region is based on the Slant TEC equation as defined by Cherniak et al. (2018), <https://doi.org/10.1007/s10291-018-0730-1>. Our results are supported by the comparison between the ROTI with TEC maps, ionograms collected at Fortaleza (FZA0M, 3°43'S, 38°32'W, dip: −15.8°), SALU, and CHPI and All-Sky imagers collected at the São João do Cariri (SJCA, 7°23'S, 36°31'W, dip: −11°) and CHPI. Additionally, we observe Equatorial Plasma Bubbles (EPBs) in the Brazilian region using the ROTI index map.

1. Introduction

Ionospheric irregularities are known to interfere in the Global Navigation Satellite System (GNSS) radio signals leading to increases in positioning errors as a function of the Total Electron Content (TEC) day-to-day variability (Hoque & Jakowski, 2008). In addition, ionospheric scintillation caused by Equatorial Plasma Bubbles (EPBs) degrades the transmission of the signal that goes from the satellite to the receiver, which can cause the loss-of-lock in the receiver (Moraes et al., 2017). Thus, the low latitude ionospheric irregularities have been widely studied in the Brazilian sector using several techniques, such as ionosonde (Abdu et al., 1982, 2003, 2012; Batista et al., 1990), Very High Frequency (VHF) radars (Abdu et al., 2009; Denardini et al., 2006), All-Sky Imagers (ASI) observations (Paulino et al., 2011; Pimenta et al., 2003), and TEC estimation (Fagundes et al., 2016; Takahashi et al., 2014, 2015). However, some aspects as the variability of EPBs, and their development, geographical coverage, and predictability are not well understood yet.

The TEC analysis is the current method that can cover all the Brazilian regions with a few blank areas, especially over the Amazon Forest (Takahashi et al., 2016), where the number of receivers is scarce. Thus, the TEC has the potential to facilitate the observations of irregularities, allowing us to measure the size and speed of propagation, among other parameters (Barros et al., 2018). We can also directly study the fluctuations in the radio signal affected by the density fluctuation in the ionosphere over a broad area, as per the analysis of the phase fluctuations in dual-frequency receivers.

There is an index based on the time rate of different phase changes in dual-frequency GNSS signals crossing the same ionospheric volume given in TECU/min (1 TECU = 10^{16} electrons/m²) named Rate Of TEC (ROT). It describes the irregularities in different length scales depending on the dual-frequency GPS signals (Pi et al., 1997). The standard deviation of the ROT is used to build another index named Rate Of TEC Index (ROTI), which does not require the Differential Code Bias (DCB) or biases to be calculated and, therefore, is used in the present study to avoid the uncertainty associated with it. The DCB (biases) refers to the TEC estimation error due to the differential satellite and instrumental receiver delay. The DCB and

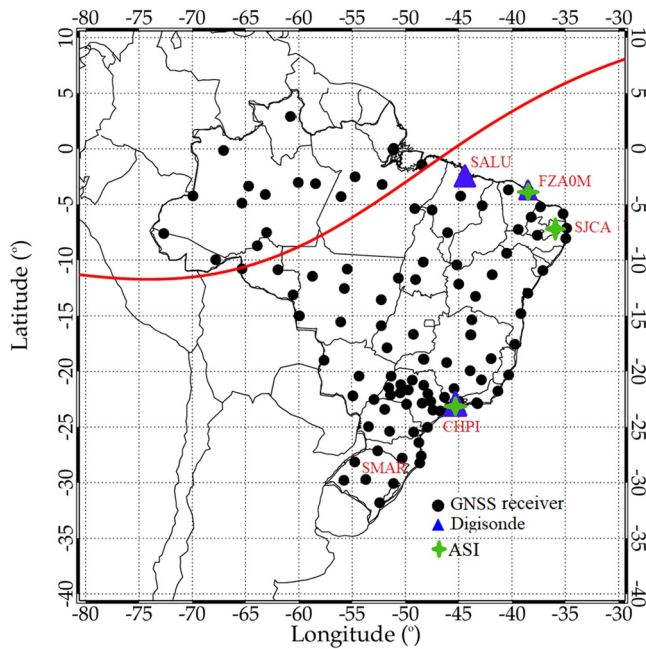


Figure 1. Map showing the locations of the Global Navigation Satellite System (GNSS) receivers (black circle), ionosondes (blue triangle), and All-Sky imagers (ASI—green cross). The red line is the magnetic equator.

TEC measurements are estimated simultaneously, and their instrumental biases may constitute significant errors in the applications, as mentioned by Sardón and Zarraoa (1997).

Currently, the ROTI is used to study plasma irregularities in some locations worldwide using different techniques. Liu, Yang, et al. (2019) analyzed the ROTI using the receivers in Asia and South America for the geomagnetic storm on March 17th, 2015. They found that ROTI values can represent the temporal evolution of ionospheric irregularities in disturbed periods. Cherniak et al. (2015) also used the ROTI maps to study ionospheric irregularities in high latitudes. They found that the ROTI map describes the development of the TEC irregularities and characterizes the ionospheric responses to auroral activity in both hemispheres. Souza and Camargo (2019) showed that ROTI could present the temporal evolution of ionospheric irregularities in the Brazilian sector. However, it was not possible to observe the propagation direction, generation, and evolution of the observed irregularities because the authors used one station only.

We found in the literature five methods used to calculate the ROTI index, which we named here as Method 1, 2, 3, 4, and 5. The details of these methods are found in Wanninger (1993, Method 1), Liu, Li, et al. (2019, Method 2), Carrano et al. (2019, Method 3), Cherniak et al. (2018, Method 4), and Liu, Yang et al. (2019, Method 5). We have compared these five methods to find which one is the most appropriate for the Brazilian sector to study the ionospheric irregularities using the ROTI in a simple way. To evaluate these techniques, we used the data collected by GNSS receivers

operating at São Luís (SALU), Cachoeira Paulista (CHPI), and Santa Maria (SMAR) during January 17th, 2015, and December 25th, 2015. Moreover, we compare our results with the ionosonde and All-Sky imager data to validate the ROTI's map's efficiency over the Brazilian region. Thereby, these two dates (January 17th, 2015, and December 25th, 2015) were used considering the TEC and ionosonde data available to confirm the presence of ionospheric irregularities.

2. Data Set

This study considers data collected from GNSS receivers, ionosondes, and All-Sky imagers to analyze the ionospheric irregularities over the selected Brazilian stations, as shown in Figure 1. In the following sections, we briefly describe each set of data used in this work.

2.1. GNSS Data and TEC Calculation

We collected the GPS receiver data of the Brazilian Network of Continuum Monitoring of GNSS System (RBMC) network driven by the Brazilian Institute of Geography and Statistics (IBGE) and the International GNSS Service (IGS).

The GPS satellites emit radio signals of dual-frequency f_1 and f_2 that allow determining the number of electrons along a vertical column with an area section of 1 m^2 that goes from the satellite to the receiver. The sub-indexes 1 and 2 correspond to the carrying frequencies band L1 (1575.42 MHz) and L2 (1227.60 MHz), respectively. Through these frequencies, we calculate the TEC derivation of the Carrier-Phase, considering an elevation angle higher than 30° , as given in Equation 1 (Mannucci et al., 1999):

$$TEC_\Phi = \frac{1}{40.3} \frac{f_1^2 f_2^2}{f_1^2 - f_2^2} \left[(\Phi_1 - \Phi_2) \right], \quad (1)$$

where f corresponds to the frequency, and Φ is the phase angle.

Also, for the calculation of the pseudorange TEC, obtaining as in Equation 2:

$$TEC_P = \frac{1}{40.3} \frac{f_1^2 f_2^2}{f_1^2 - f_2^2} [(P_2 - P_1)], \quad (2)$$

where P_1 and P_2 are the pseudorange corresponds to the f_1 and f_2 , respectively.

The relative TEC is obtained according to Equation 3:

$$TEC = TEC_{\Phi} + \langle TEC_P - TEC_{\Phi} \rangle, \quad (3)$$

where $\langle \rangle$ is the average over the day.

In our methodology, the main goal is to calculate the TEC most simply. Thereby, the satellites/receivers' biases and phase ambiguity were not included in the TEC calculation and, consequently, the ROTI.

The vertical TEC (VTEC) by applying a mapping function shown in Equation 4:

$$VTEC = TEC \left[1 - \left(\frac{R_e \cos(\theta)}{R_e + h_I} \right) \right]^{-\frac{1}{2}}, \quad (4)$$

where R_e is the Earth radius, h_I is the height of the Ionospheric Pierce Point (IPP) (in this work we consider equal to 350 km), θ is the angle of elevation in radians, and the TEC is given in TEC units, in which 1 TECU equals 10^{16} electrons/m². More details about the TEC calculation are given in Takahashi et al. (2016).

2.2. Ionosonde Data

The ionosonde is an ionospheric radar that operates in variable high frequency (HF) used to investigate the ionosphere regions (Abdu et al., 2010). The data collected are the electromagnetic wave echoes reflected by the ionospheric layers of corresponding electron density to the transmitted signal frequency. These echoes are registered in graphics (ionograms) of the transmitted frequency versus virtual height ($h'F$), which provides the different regions' electron density profiles in the ionosphere (Reinisch et al., 2009). The data set of the ionosondes is found in the Brazilian Space Weather Study and Monitoring Program (Embrace) Digisonde Network (<http://www2.inpe.br/climaespacial/portal/>), and the details about their characteristics are in Batista et al. (1996).

In this work, we use ionosonde data acquired in SALU, FZA0M, and CHPI to examine the plasma irregularity presence observed in the ROTI index. The occurrence of irregularities in the F region is shown as "Spread-F" in ionosonde data characterized by signal scattering regions. These irregularities are aligned along the Earth's magnetic field, and they are associated with plasma bubbles (Spencer, 1955).

2.3. All-Sky Imager

The All-Sky imager (ASI) is used for observations of airglow emissions in the mesosphere and ionosphere from the Hydroxyl (OH 700–900 nm) and Atomic Oxygen (OI 630 nm), respectively. This equipment has a fisheye lens, with a field of view of $\sim 180^\circ$, filters, lenses, and a CCD camera (1024 x 1024 pixels) (Paulino et al., 2011; Wrasse et al., 2006). The red line emission image covers a horizontal extension of 1,600 km (at the zenith angle of 75°) at an altitude of 250 km (Takahashi et al., 2015).

In this study, the ASI data from São João do Cariri and CHPI were used to confirm the occurrences of plasma bubbles, enabling the ROTI validation.

3. Methodology

As mentioned before, we use the ROTI index to observe the ionospheric irregularities. The calculation of ROTI is based on the ROT, defined in Equation 5 (Pi et al., 1997):

Table 1
The Five Methods Used in This Work Showing the ROT, Sampling Rate, Scale, and Elevation

Method	ROT	Rate	Elevation	Reference
1	VTEC	5 min	>20°	Wanninger (1993)
2	STEC	5 min	–	Liu, Li, et al. (2019)
3	VTEC	1 or 5 min	>30°	Carrano et al. (2019)
4	STEC	5 min	>30°	Cherniak et al. (2018)
5	STEC	5 min	>30°	Liu, Yang, et al. (2019)

$$ROT = \frac{TEC_{t_2} - TEC_{t_1}}{t_2 - t_1} = \frac{\Delta TEC}{\Delta t}, \quad (5)$$

where t is the time and $TEC_{t_{1,2}}$ is the value corresponding to the TEC at time t_1 and t_2 . Notice that the ROT is based on the difference of the TEC values in two points. The $ROTI$ was based on the standard deviation of ROT with 5-minutes time interval, as in Equation 6 (Pi et al., 1997).

$$ROTI = \sqrt{\langle ROT^2 \rangle - \langle ROT \rangle^2}, \quad (6)$$

where $\langle ROT \rangle$ denotes arithmetic averaging ROT during N epoch.

In the present study, we used the TEC calculated by Seemala and Valladares (2011) to obtain the $ROTI$ in Equation 6. This technique was considered as a reference because it is a reliable and well-established scientific community method. After that, we tested five different methods to calculate the $ROTI$ index. It is important to mention here that the methodology used in this study refers to the relative TEC .

3.1. Analysis of the Different Techniques for $ROTI$ Calculation

Table 1 shows the five methods and their main characteristics used to derive the $ROTI$ index in this analysis. Some important information is described in this table, such as sample rate, elevations, and the corresponding reference. Most of the studies used the 5-min sampling rate, except the technique in Carrano et al. (2019) that allows a 1-min sample. Wanninger (1993) and Carrano et al. (2019) used the vertical absolute TEC data, that is, including satellite/receive biases, while the others used the slant TEC ($STEC$). On the other hand, Liu, Li, et al. (2019) used the Carrier-Phase TEC with biases projected in the vertical. As mentioned before, the $ROTI$ is calculated using Equation 6 (Pi et al., 1997). Therefore, the main difference between these techniques is only related to the TEC calculation. Note that the TEC adopted in this study was aforementioned in the methodology.

3.1.1. Method 1

Method 1 ($M1$) calculates the Rot_{M1} index from the TEC , as shown in Equation 7 (Wanninger, 1993).

$$Rot_{M1}(t_2) = TEC(t_2) - TEC(t_1), \quad (7)$$

where t is the time.

The $ROTI_{M1}$ (Equation 8) is obtained from the calculation using Equation 6 applied to Method 1 ($M1$).

$$ROTI_{M1} = \sqrt{\langle Rot_{M1}^2 \rangle - \langle Rot_{M1} \rangle^2}, \quad (8)$$

where $\langle \rangle$ is the average.

3.1.2. Method 2

Method 2 ($M2$) calculates the $ROTI_{M2}$ index using the formalisms proposed by Liu, Li, et al. (2019), as shown in Equations 5 and 9.

$$ROTI_{M2} = \sqrt{\frac{1}{N} \sum_{j=1}^N (ROT_j - ROT_{aver})^2}, \quad (9)$$

where ROT_{aver} indicates the average of the ROT .

3.1.3. Method 3

Method 3 ($M3$) is defined by Carrano et al. (2019), the $ROTI_{M3}$ index is calculated according to Equation 10.

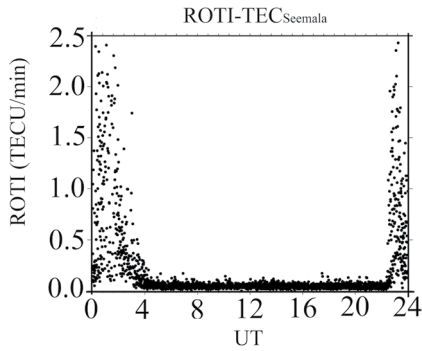


Figure 2. The $ROTI-TEC_{Seemala}$ shows the plasma irregularities in the nighttime period for SALU station on December 25th, 2015.

$$ROTI^2_{M3}(\delta t) = \left\langle \frac{|TEC(t + \delta t) - TEC(\delta t)|}{\delta t} \right\rangle, \quad (10)$$

where δt is the time variation, and the $\langle \rangle$ is the moving average in 5-min.

3.1.4. Method 4

Method 4 (M4) uses $sTEC_{M4}$ according to Equation 11 (Cherniak et al., 2018).

$$sTEC_{M4} = \left(\frac{L_1}{f_1} - \frac{L_2}{f_2} \right) \frac{f_1^2 f_2^2}{f_1^2 - f_2^2} \frac{c}{k}, \quad (11)$$

the frequencies values are $f_1 = 1575.42$ MHz and $f_2 = 1227.60$ MHz, the L_1 and L_2 are the carrying frequencies band corresponding to frequencies 1 and 2, the parameter k is $40.3 \text{ m}^3/\text{s}^2$, and c is the speed of light in the vacuum. The ROT_{M4} index, follows the same formalism presented in Equation 5.

The ROT_{M4} is then obtained from the calculation using Equation 6 applied to this Method 4 (M4).

3.1.5. Method 5

Method 5 (M5) is defined by Liu, Yang, et al. (2019), and it used the TEC_{M5} data obtained through Equation 12.

$$TEC_{M5} = \frac{1}{40.3} \left(\frac{f_1^2 f_2^2}{f_1^2 - f_2^2} \right) \left[(\lambda_2 L_2 - \lambda_1 L_1) - [(\lambda_2 N_2 - \lambda_1 N_1) + (d_2 - d_1)] \right], \quad (12)$$

where the f_1 , f_2 , L_1 and L_2 were defined in Method 4, λ is the wavelength, N is the phase ambiguity, d is the phase delay between the satellite and receiver (biases).

Thus, the ROT_{M5} is calculated according to Equation 13.

$$ROT_{M5} = C \frac{\left[(\lambda_2 L_2(i) - \lambda_1 L_1(i)) - (\lambda_2 L_2(i-1) - \lambda_1 L_1(i-1)) \right]}{(t_i - t_{i-1})}, \quad (13)$$

where C is $\frac{1}{40.3} \left(\frac{f_1^2 f_2^2}{f_1^2 - f_2^2} \right)$, t is the time, and i is the first position. Notice that the terms $(\lambda_2 N_2 - \lambda_1 N_1)$ and $(d_2 - d_1)$ are canceled. Therefore, after determining the TEC, it is possible to calculate the ROT_{M5} through Equation 6 applied to Method 5 (M5).

4. Results

This work aims to find an acceptable method for ROTI calculation over the Brazilian sector since this parameter is very suitable for identifying the plasma irregularities. First, we estimated the ROTI (Equation 6) using the TEC calculation given in Seemala and Valladares (2011) named $ROTI-TEC_{Seemala}$. The $ROTI-TEC_{Seemala}$ data is shown in Figure 2 for the equatorial station SALU on December 25th, 2015. The vertical scale is in TECU/min, meaning that the irregularity occurs for high values of this index. We observe expressive values between 00:00 and 04:00 UT (UT = LT + 3) and between 22:00 and 24:00 UT. This behavior is a strong indication of the plasma irregularities in the nighttime period. Also, the ROTI has low values during the daytime (<1 TECU/min).

Additionally, Figure 3 shows the ROTI index using the five methods for the same station (SALU) on December 25th, 2015. We observed that the results of Methods 1 (a), 2 (b), and 3 (c) show different behavior when compared with the $ROTI-TEC_{Seemala}$ (Figure 2). Using Figure 2 as a reference, we notice that Methods 1 to 3 are different, and the results presented unrealistic values during the daytime. Thus, these methods

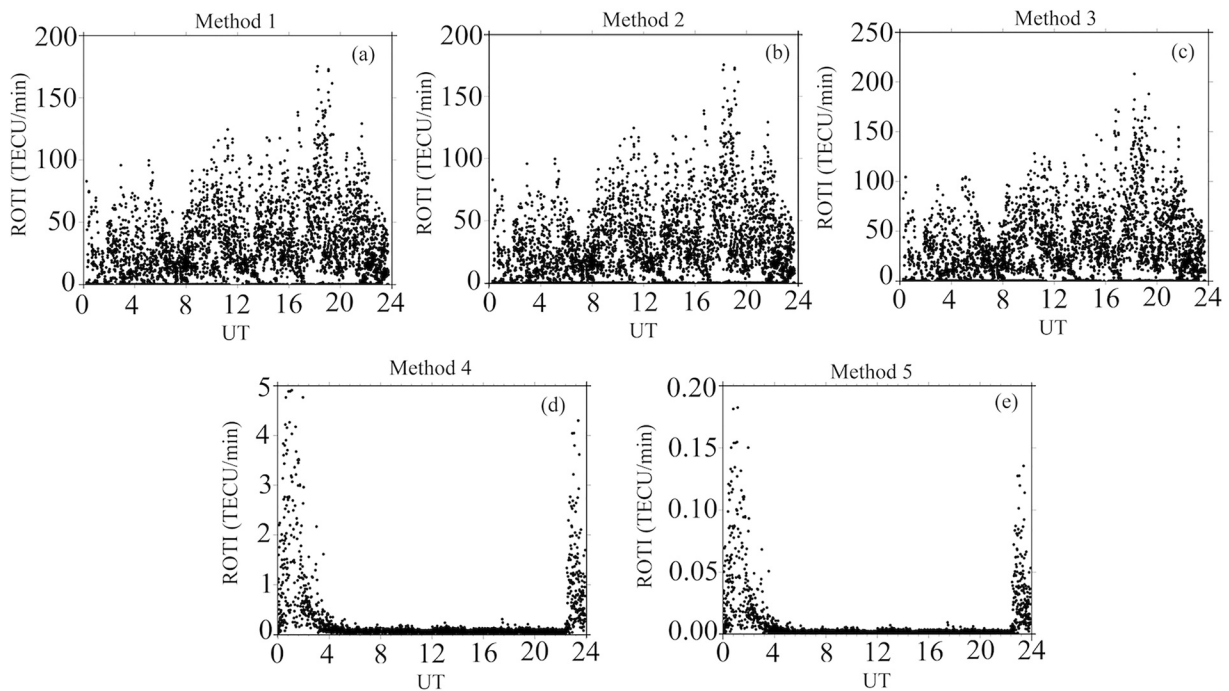


Figure 3. Rate Of TEC (ROTI) index using the different methods calculated for SALU on December 25th, 2015.

can be regarded as inappropriate in this study. In fact, this means that these methods do not work when we apply the relative TEC equation since these methods require the use of absolute TEC. On the other hand, we observe a similarity in the results of Methods 4 (d) and 5 (e) with the ROTI-TEC_{Seemala}. These two methods are based only on the carrier phase TEC without biases, making their use promising for the methodology proposed in this study. As the ionospheric layers are magnetically connected during the daytime due to the significant E region conductivity, it is difficult to make the appearance of plasma irregularities in the F region at these times (Abdu, 2005). During the nighttime, the high values can also be referred to as plasma irregularities.

We performed a correlation between these five techniques with the ROTI-TEC_{Seemala} for a more detailed analysis shown in Figure 4. The correlation coefficients (R), linear (b), and angular (a) coefficients are summarized in Table 2. As expected, Methods 1, 2, and 3 present a small angular coefficient, meaning there is no linear dependence. This fact occurs because Methods 1, 2, and 3 did not include receiver and satellite biases. Therefore, the TEC values become greater than the ROTI values calculated by TEC_{Seemala}. Therefore, these three methods depend on satellite and receiver biases to obtain adequate ROTI values.

Methods 4 and 5 show a good correlation with the $R > 0.8$. In Figures 4d and 4e, we notice that the correlations are similar between these methods. Thus, both methods are good enough to observe the irregularities in the equatorial region. The ideal scenario in this work, meaning that the ROTI from each method has the same behavior as the ROTI reference, would be reached if the values from both methods described a straight line ($x = y$) in the scatter plot with a very high correlation coefficient ($R \sim 1$).

Table 2 shows the R , b , and a coefficients for each method. It is possible to observe that Methods 4 and 5 had a good correlation ($0.8 < |R| < 0.9$), and the linear and angular coefficients of Method 4 were the ones that came closest to an ideal case (Press et al., 2002; Bevington & Robinson, 2003). Finally, although Methods 4 and 5 have resembled, we use Method 4 because the correlation is higher ($R = 0.88$), and its mathematical formulation is simple. Also, the ROTI index scale is almost the same as the ROTI-TEC_{Seemala}.

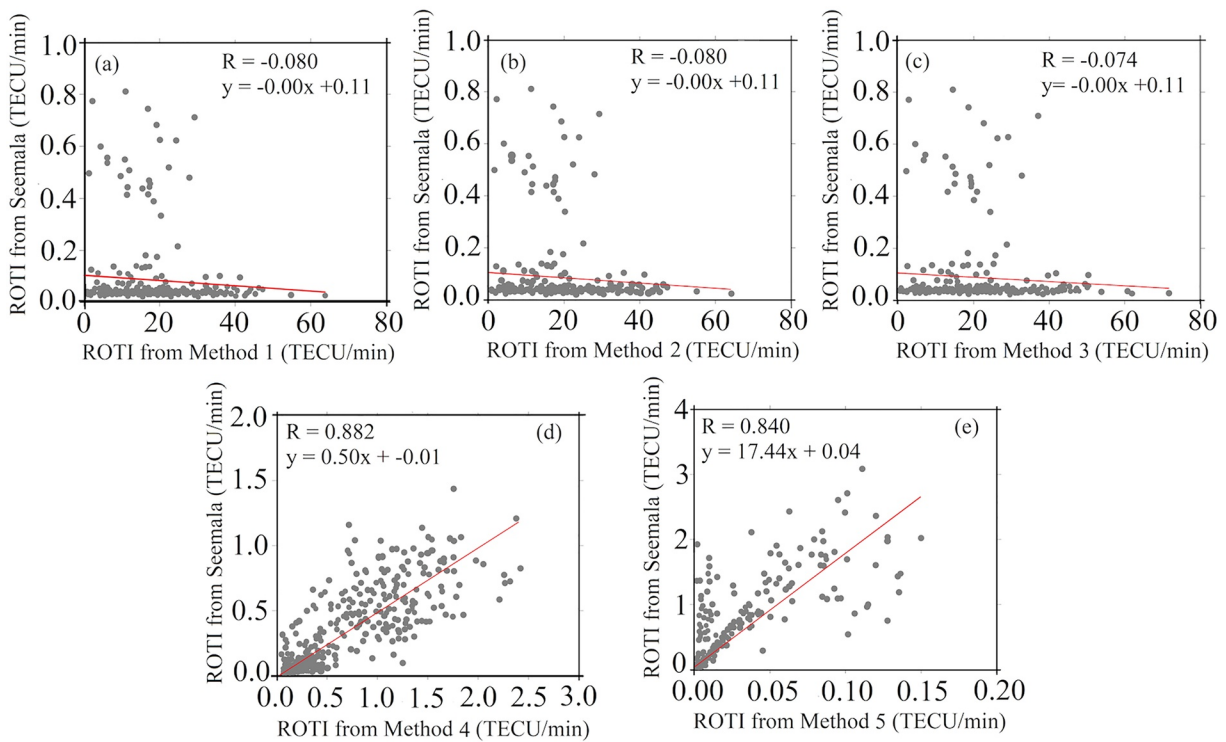


Figure 4. Correlation between the methods analyzed in this study and the ROTI-TEC_{Seemala} for (a) Method 1, (b) Method 2, (c) Method 3, (d) Method 4, and (e) Method 5.

5. Case Studies of Ionospheric Irregularities Using the ROTI Index Over the Brazilian Sector

Figure 5 shows the time variation of the ROTI index on the same day used before (December 25th, 2015) for SALU (a) and the other two low latitudes regions, CHPI (b) and SMAR (c). Here, we used Method 4 as described above. As mentioned in Pi et al. (1997), the ROTI values greater than 2 TECU/min could be associated with ionospheric irregularities. Our results show the ROTI index values greater than 5 TECU/min in the nighttime over the SALU region, whereas, in CHPI and SMAR, the ROTI index is less than 1 TECU/min. Thus, the ionospheric irregularities may have generated at the equatorial region, and no ionospheric irregularities were observed at low latitudes.

We have used a multi-instrumental analysis to identify the irregularity presence in the equatorial sector and the structure type. Figure 6 shows the ROTI map (a), the TEC map over the Brazilian regions (b), and an ionogram at the night period (23:40 UT) in SALU (c). Also, to compare with the low latitude station, we included an ionogram in the same hour for CHPI (d). Unfortunately, we have no digisonde data for the SMAR station in this period. The TEC map shows the well-known Equatorial Ionization Anomaly, composed of the peaks of density away from the magnetic equator (Nogueira et al., 2011). The ROTI map (a) and the TEC map (b) show the low density around the magnetic equator line (red arrow) refers to the plasma bubble. In the ionogram over SALU, we observe the Spread-F presence, indicating the possible plasma bubbles occurrence. Therefore, the plasma irregularity presence in SALU agrees with the ROTI index's high values. Additionally, no Spread-F was observed at CHPI, also agreeing with the ROTI index results.

We performed the same analysis for the three same regions, which are SALU (a), CHPI (b), and SMAR (c), on January 17th, 2015, shown in Figure 7. On this day, we observe increases in night hours in all stations

Table 2
The Correlation Coefficient (R), Linear (b), and Angular (a) Coefficients for Each Method Used in This Work

Figure	Method	Correlation coefficient (R)	Angular (a)	Linear (b)
A	1	0.080	-0.00	0.11
B	2	0.080	-0.00	0.11
C	3	0.074	-0.00	0.11
D	4	0.882	0.50	-0.01
E	5	0.840	17.44	0.04

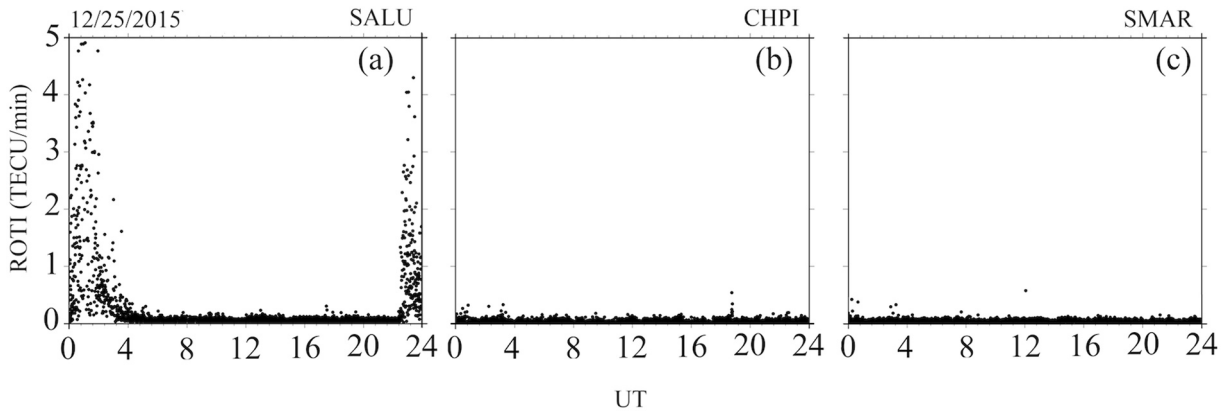


Figure 5. Rate Of TEC (ROTI) index for SALU (a), CHPI (b), and SMAR (c) stations on December 25th, 2015.

analyzed. In SALU, the ROTI index reaches 3 TECU/min around 00:00–04:00 UT and 23:00–24:00 UT. In CHPI, the ROTI index showed values greater than 3 TECU/min between 00:00–04:00 UT and from 23:00 to 24:00 UT. Furthermore, the ROTI index reaches values greater than 1 TECU/min in SMAR between 00:00 and 04:00 UT.

As previously seen, the studies with ROTI and ionosonde in situ do not provide us with the type of irregularity. Thereby, we have built ROTI maps with hundreds of GNSS receivers in the Brazilian sector to identify and characterize EPBs. Additionally, the ROTI maps are independent of other equipment. In Figure 8, we have the ROTI Map (a), the TEC Map (b), OI 630 nm image in SJCA (c), and CHPI (d). Additionally, we show an ionogram over FZA0M (e) and CHPI (f) on January 17th, 2015. In this figure, the ROTI map and the TEC map show plasma bubbles over the EIA’s Southern crest extending at least over -25° S (red arrow). Already the OI 630 nm image shows a strong plasma bubble in both stations. Lastly, we have observed the Spread-F in both stations during the nighttime. All these observations are good correlated to the ROTI index’s high values, confirming that these irregularities are plasma bubbles.

We do not have any additional instruments over SMAR to compare our results. However, as proposed in Seba et al. (2018) for West Africa, the expressive ROTI values can be plasma bubbles. Thus, we strongly believed that the significant ROTI values (higher than 4 TECU/min) are related to the SMAR’s plasma bubbles presence. Therefore, we concluded that even though there was no ionosonde available in the SMAR station to confirm the appearance of spread F in this date, the ROTI index is sufficient to prove the presence of a

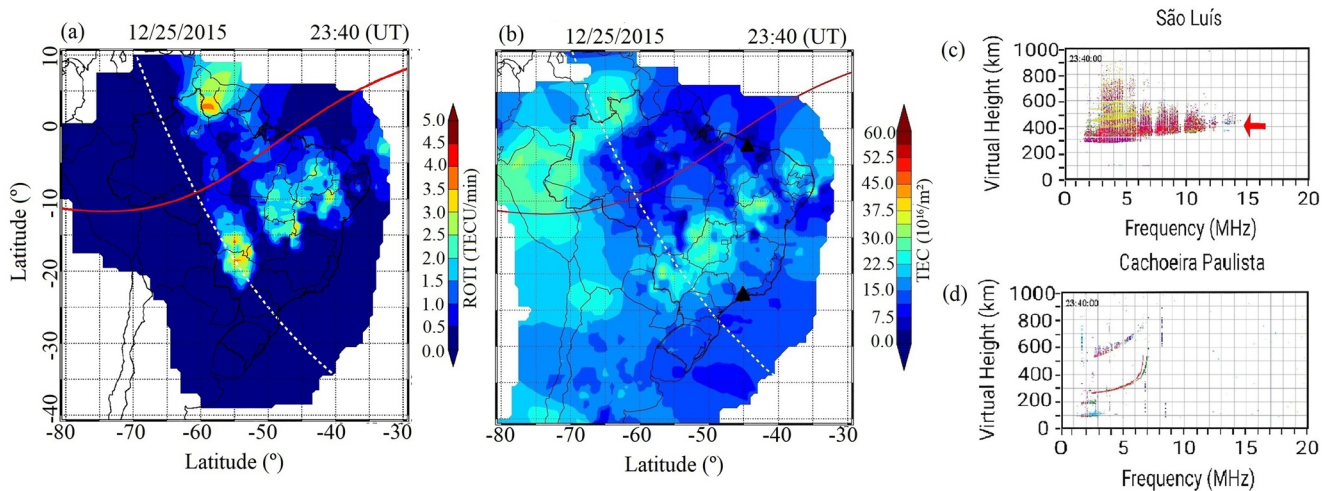


Figure 6. (a) Map of Rate of TEC Index (ROTI), (b) Map of Total Electron Content (TEC), (c) Ionogram in SALU, and (d) Ionogram in CHPI on December 25th, 2015, at 23:40 UT.

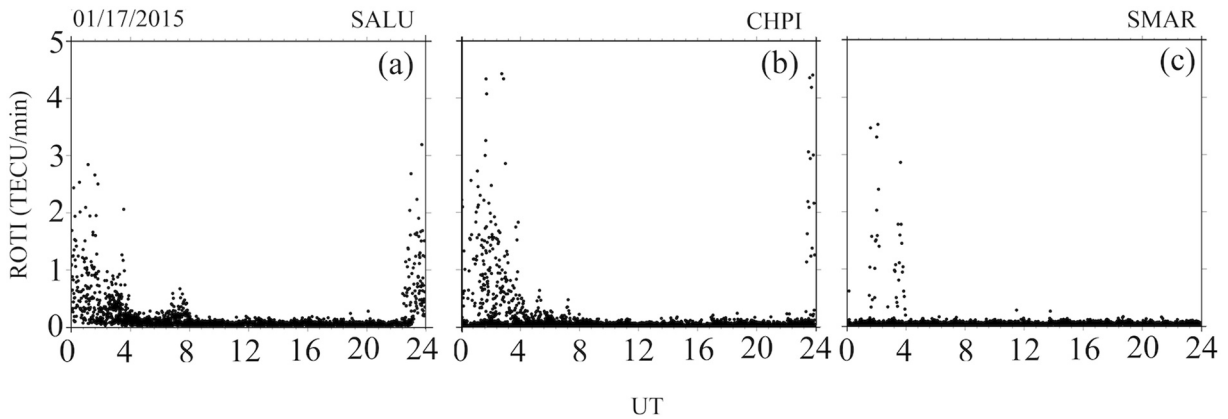


Figure 7. Map of Rate Of TEC (ROTI) index for SALU (a), CHPI (b), and SMAR (c) stations for January 17th, 2015.

plasma bubble at low and equatorial latitudes. In addition, this is a period of the high occurrence of plasma bubbles in the Brazilian region (Barros et al., 2018).

Figure 9 shows the TEC map (a), the ROTI map using the $TEC_{seemala}$ (b), and the Method 4 used in our analysis (c) over the Brazilian region on January 17th, 2015. We see four well-defined plasma bubble structures on the ROTI maps (Figures 9b and 9c), with propagation direction to the eastward, and it reaches 30°S. We can also see more details of the plasma bubble structures than the TEC map (Figure 9a). Therefore, we can conclude that the ROTI maps are better than the TEC maps to visualize these irregularities.

The linear correlation coefficient was also calculated between the ROTI- $TEC_{seemala}$ maps (Figure 9b) and the ROTI maps (Figure 9c). We obtained an average correlation coefficient of ~ 0.993 . This correlation is greater than that obtained previously in Table 2, Method 4, which was 0.88. It was possible because the matrix generated for the maps are results of the ROTI of several stations and obtained after smoothing. We have obtained a significant similarity between the two methodologies used.

Finally, this study shows that the ROTI index using Method 4 is very good to observe the irregularities in the Brazilian region. The TEC depletion, the presence of the plasma bubble in the ASI, and the Spread-F occurrence in the ionograms corroborate that the ROTI index adopted in this study can potentially alert the presence of plasma bubbles in the Brazilian sector. The ROTI index also has the advantage of being a local index to indicate plasma irregularities that affect extensive ionospheric error range for a single-frequency positioning system. In addition, we strongly believe that the ROTI technique is a good method to study the peculiarities that occurs over the Brazilian region, being able to have reliability even when there are no other equipment measurements in the studied regions. Indeed, it may be a potential parameter for space weather applications.

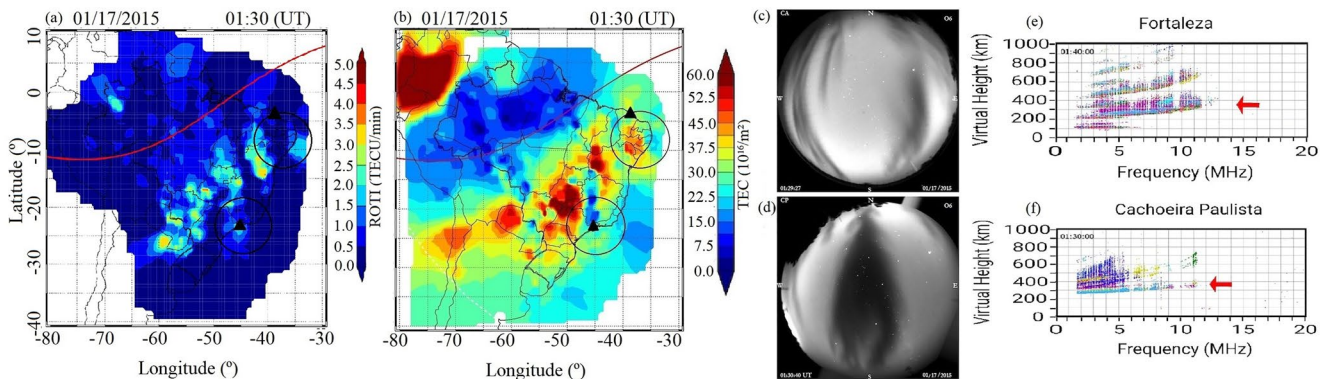


Figure 8. Plasma bubbles observed in (a) Map of Rate Of TEC (ROTI), (b) Map of Total Electron Content (TEC), (c) All-sky imager in São João do Cariri, and (d) CHPI, (e) the ionograms over Fortaleza and (f) CHPI station, on January 17th, 2015.

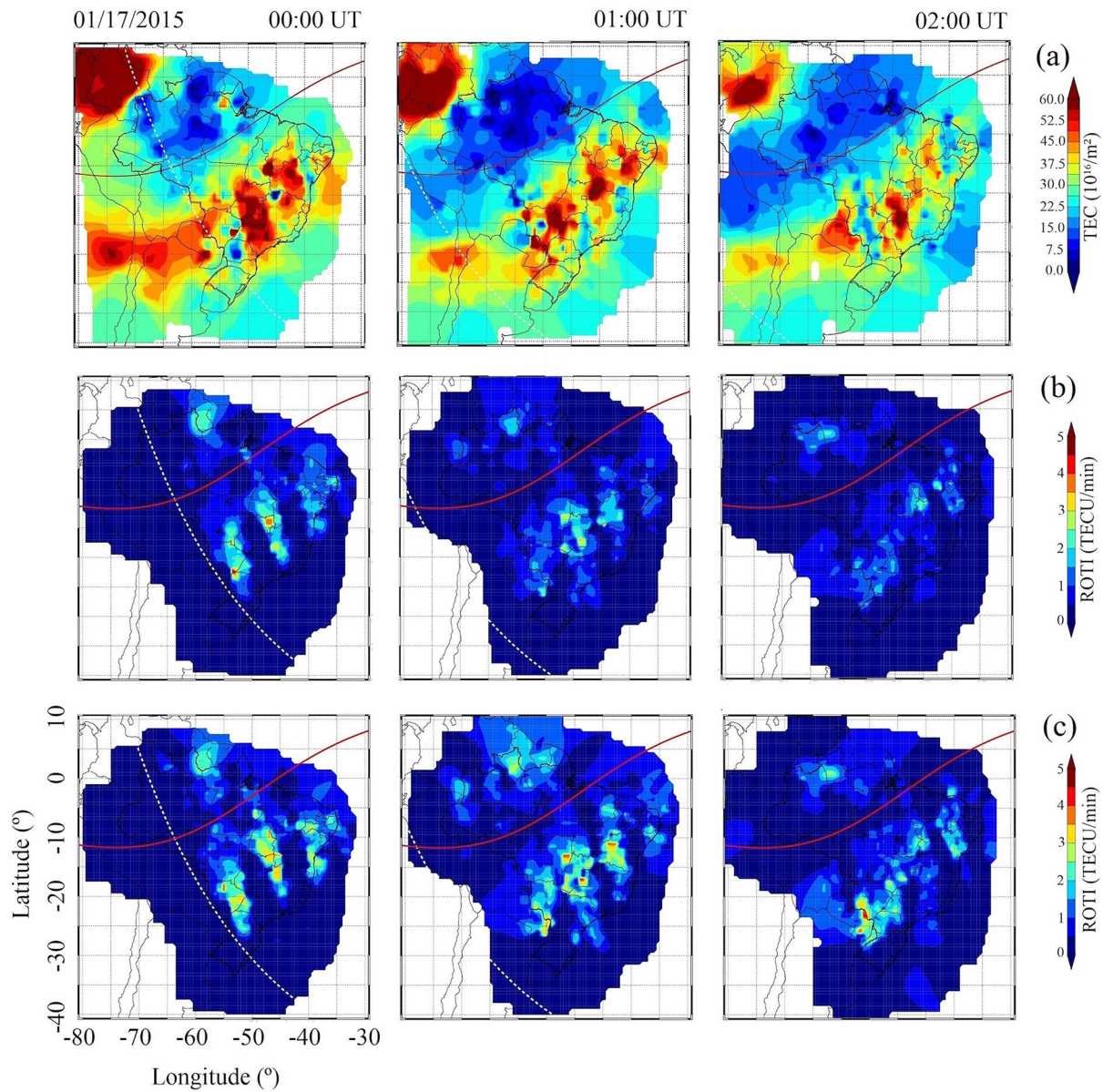


Figure 9. Total Electron Content (TEC) map (a), ROTI map with a TEC_{Seemala} (b), and ROTI map (c), at 00:00, 01:00, and 02:00 UT, on January 17th, 2015.

6. Conclusions

In this study, we have compared five different approaches for ROTI calculations to find the best and simple method for ROTI in the Brazilian sector. Then, we found the most appropriate method to identify the ionospheric plasma irregularities, such as plasma bubbles over the equatorial latitudes. Our main findings are summarized below.

1. This study shows that Method 4 is the most appropriate to obtain the ROTI index with a simple methodology to analyze irregularities in the Brazilian sector. On the other hand, Methods 1, 2, and 3 do not present satisfactory results since the applied methodology did not consider the TEC calculation biases, showing that these three methods require these biases.
2. The methodology presented by Cherniak et al. (2018) called Method 4 in our work presented the highest correlation to $ROTI-TEC_{\text{Seemala}}$.

3. We have compared the ROTI irregularities observed with Method 4 with observations from ionosondes, ASI, and TEC Maps. In all cases analyzed, the plasma bubbles presence has been observed in different instruments since the ROTI index has reached values greater than 1 TECU/min.
4. Finally, we built the ROTI index maps, which are considered a great method to classify and characterize the ionospheric irregularities. Also, these maps are independent of other techniques to identify plasma bubbles.

Acknowledgments

The authors thank the Embrace/INPE Space Weather Program for providing the TEC maps, ionograms, and images by All-Sky imager (<http://www.inpe.br/spaceweather>), the IBGE for providing the satellite data (Rinex) (<https://www.ibge.gov.br/geociencias/downloads-geociencias.html>) and the program to calculate the TEC (<https://seemala.blogspot.com/>). C. S. Carmo thanks CNPq/MCTIC (Grant 141935/2020-0). C. M. Denardini thanks CNPq/MCTIC (Grant 303643/2017-0). C. A. O. B. Figueiredo thanks Fundação de Amparo à Pesquisa do Estado de São Paulo (FAPESP) (Grant 2018/09066-8). L. C. A. Resende thanks the China-Brazil Joint Laboratory for Space Weather (CBJLSW), National Space Science Center (NSSC), Chinese Academy of Sciences (CAS) for supporting her Postdoctoral fellowship. G. A. S. Picanço thanks CAPES/MEC (Grant 88887.351778/2019-00). P. F. Barbosa Neto thanks CAPES/MEC (Grant 1622967). J. Moro thanks the China-Brazil Joint Laboratory for Space Weather (CBJLSW), National Space Science Center (NSSC), Chinese Academy of Sciences (CAS) for supporting his Postdoctoral fellowship, and the CNPq/MCTIC (Grant 429517/2018-01). S. S. Chen thanks CAPES/MEC (Grant 88887.362982/2019-00).

References

- Abdu, M. A. (2005). Equatorial ionosphere–thermosphere system: Electrodynamics and irregularities. *Advances in Space Research*, 35, 771–787. <https://doi.org/10.1016/j.asr.2005.03.150>
- Abdu, M. A., Batista, I. S., Brum, G. M., MacDougall, J. W., Santos, A. M., de Souza, J. R., & Sobral, J. H. A. (2010). Solar flux effects on the equatorial evening vertical drift and meridional winds over Brazil: A comparison between observational data and the IRI model and the HWM representations. *Advances in Space Research*, 46(8), 1078–1085. <https://doi.org/10.1016/j.asr.2010.06.009>
- Abdu, M. A., Batista, I. S., Reinisch, B. W., MacDougall, J. W., Kherani, E. A., & Sobral, J. H. A. (2012). Equatorial range spread F echoes from coherent backscatter, and irregularity growth processes, from conjugate point digital ionograms. *Radio Science*, 47(06), 1–8. <https://doi.org/10.1029/2012RS005002>
- Abdu, M. A., Batista, I. S., Takahashi, H., MacDougall, J., Sobral, J. H., Medeiros, A. F., & Trivedi, N. B. (2003). Magnetospheric disturbance induced equatorial plasma bubble development and dynamics: A case study in Brazilian sector. *Journal of Geophysical Research*, 108(A12), 1449. <https://doi.org/10.1029/2002ja009721>
- Abdu, M. A., De Medeiros, R. T., & Sobral, J. H. A. (1982). Equatorial spread F instability conditions as determined from ionograms. *Geophysical Research Letters*, 9(6), 692–695. <https://doi.org/10.1029/GL0091006p00692>
- Abdu, M. A., Kherani, E. A., Batista, I. S., De Paula, E. R., Fritts, D. C., & Sobral, J. H. A. (2009). Gravity wave initiation of equatorial spread F/plasma bubble irregularities based on observational data from the SpreadFEX campaign. *Annales Geophysicae*, 27(7), 2607–2622. <https://doi.org/10.1029/2002JA009721>
- Barros, D., Takahashi, H., Wrasse, C. M., & Figueiredo, C. A. O. (2018). Characteristics of equatorial plasma bubbles observed by TEC map based on ground-based GNSS receivers over South America. In *Annales geophysicae*. (Vol. 36, pp. 91–100). Copernicus GmbH. <https://doi.org/10.5194/angeo-36-91-2018>
- Batista, I. S., Abdu, M. A., De Medeiros, R. T., & De Paula, E. R. (1996). Comparison between IRI predictions and digisonde measurements at low latitude station. *Advances in Space Research*, 18(6), 49–52. [https://doi.org/10.1016/0273-1177\(95\)00899-3](https://doi.org/10.1016/0273-1177(95)00899-3)
- Batista, I. S., Abdu, M. A., & Medrano, R. A. (1990). Magnetic activity effects on range type spread-F and vertical plasma drifts at Fortaleza and Huancayo as studied through ionosonde measurements and theoretical modelling. *Annales Geophysicae*, 8, 357–364.
- Bevington, P. R., & Robinson, D. K. (2003). *Data reduction and error analysis*. New York: McGraw Hill.
- Carrano, C. S., Groves, K. M., & Rino, C. L. (2019). On the relationship between the rate of change of total electron content index (ROTI), irregularity strength (CkL), and the scintillation index (S4). *Journal of Geophysical Research: Space Physics*, 124(3), 2099–2112. <https://doi.org/10.1029/2018JA026353>
- Cherniak, I., Krankowski, A., & Zakharenkova, I. (2018). ROTI Maps: A new IGS ionospheric product characterizing the ionospheric irregularities occurrence. *GPS Solutions*, 22(3), 69. <https://doi.org/10.1007/s10291-018-0730-1>
- Cherniak, I., Zakharenkova, I., & Redmon, R. J. (2015). Dynamics of the high-latitude ionospheric irregularities during the 17 March 2015 St. Patrick's Day storm: Ground-based GPS measurements. *Space Weather*, 13(9), 585–597. <https://doi.org/10.1002/2015SW001237>
- Denardini, C. M., Abdu, M. A., De Paula, E. R., Wrasse, C. M., & Sobral, J. H. A. (2006). VHF radar observations of the dip equatorial E-region during sunset in the Brazilian sector. *Annales Geophysicae*, 24, 1617–1623. <https://doi.org/10.5194/angeo-24-1617-2006>
- Fagundes, P. R., Cardoso, F. A., Fejer, B. G., Venkatesh, K., Ribeiro, B. A. G., & Pillat, V. G. (2016). Positive and negative GPS-TEC ionospheric storm effects during the extreme space weather event of March 2015 over the Brazilian sector. *Journal of Geophysical Research: Space Physics*, 121(6), 5613–5625. <https://doi.org/10.1002/2015JA022214>
- Hoque, M. M., & Jakowski, N. (2008). Estimate of higher order ionospheric errors in GNSS positioning. *Radio Science*, 43, RS5008. <https://doi.org/10.1029/2007RS003817>
- Liu, Y., Li, Z., Fu, L., Wang, J., Radicella, S. M., & Zhang, C. (2019a). Analyzing ionosphere TEC and ROTI responses on 2010 August high speed solar winds. *IEEE Access*, 7, 29788–29804. <https://doi.org/10.1109/ACCESS.2019.2897793>
- Liu, Z., Yang, Z., Xu, D., & Morton, Y. J. (2019b). On inconsistent ROTI derived from multiconstellation GNSS measurements of globally distributed GNSS receivers for ionospheric irregularities characterization. *Radio Science*, 54(3), 215–232. <https://doi.org/10.1029/2018RS006596>
- Mannucci, A. J., Iijima, B. A., Lindqwister, U. J., Pi, X., Sparks, L., & Wilson, B. D. (1999). GPS and ionosphere. In Stone, W. R. (Ed.), *Review of radio science 1996–1999* (pp. 625–665). Ghent, Belgium: International Union of Radio Science.
- Moraes, A. O., Costa, E., Abdu, M. A., Rodrigues, F. S., de Paula, E. R., Oliveira, K., & Perrella, W. J. (2017). The variability of low-latitude ionospheric amplitude and phase scintillation detected by a triple-frequency GPS receiver. *Radio Science*, 52, 439–460. <https://doi.org/10.1002/2016RS006165>
- Nogueira, P. A. B., Abdu, M. A., Batista, I. S., De Siqueira, P. M., & de Siqueira, P. M. (2011). Equatorial ionization anomaly and thermospheric meridional winds during two major storms over Brazilian low latitudes. *Journal of Atmospheric and Solar-Terrestrial Physics*, 73(11–12), 1535–1543. <https://doi.org/10.1016/j.jastp.2011.02.008>
- Paulino, I., Medeiros, A. F. D., Buriti, R. A., Takahashi, H., Sobral, J. H. A., & Gobbi, D. (2011). Plasma bubble zonal drift characteristics observed by airglow images over Brazilian tropical region. *Revista Brasileira de Geofísica*, 29(2), 239–246. <https://doi.org/10.1590/S0102-261X2011000200003>
- Pi, X., Mannucci, A. J., Lindqwister, U. J., & Ho, C. M. (1997). Monitoring of global ionospheric irregularities using the Worldwide GPS Network. *Geophysical Research Letters*, 24(18), 2283–2286. <https://doi.org/10.1029/97GL02273>
- Pimenta, A. A., Bittencourt, J. A., Fagundes, P. R., Sahai, Y., Buriti, R. A., Takahashi, H., & Taylor, M. J. (2003). Ionospheric plasma bubble zonal drifts over the tropical region: A study using OI 630nm emission all-sky images. *Journal of Atmospheric and Solar-Terrestrial Physics*, 65(10), 1117–1126. [https://doi.org/10.1016/S1364-6826\(03\)00149-4](https://doi.org/10.1016/S1364-6826(03)00149-4)

- Press, W. H., Teuskolsky, S. A., Vetterling, W. T., & Flannery, B. P. (2002). *Numerical recipes in C: The art of scientific computing* (2nd ed.). Cambridge: Cambridge University Press.
- Reinisch, B. W., Galkin, I. A., Khmyrov, G. M., Kozlov, A. V., Bibl, K., Lisysyan, I. A., et al. (2009). New Digisonde for research and monitoring applications. *Radio Science*, *44*, RS0A24. <https://doi.org/10.1029/2008RS004115>
- Sardón, E., & Zarraoa, N. (1997). Estimation of total electron content using GPS data: How stable are the differential satellite and receiver instrumental biases? *Radio Science*, *32*(5), 1899–1910. <https://doi.org/10.1029/97RS01457>
- Seba, E. B., Nigussie, M., & Moldwin, M. B. (2018). The relationship between equatorial ionization anomaly and nighttime equatorial spread F in East Africa. *Advances in Space Research*, *62*(7), 1737–1752. <https://doi.org/10.1016/j.asr.2018.06.029>
- Seemala, G. K., & Valladares, C. E. (2011). Statistics of total electron content depletions observed over the South American continent for the year 2008. *Radio Science*, *46*(5), RS5019. <https://doi.org/10.1029/2011RS004722>
- Souza, A. L. C. D., & Camargo, P. D. O. (2019). Comparison of GNSS indices, ionosondes and all-sky imagers in monitoring the ionosphere in Brazil during quiet and disturbed days. *Boletim de Ciências Geodésicas*, *25*. <https://doi.org/10.1590/s1982-21702019000s00005>
- Spencer, M. (1955). The shape of irregularities in the upper ionosphere. In *Proceedings of the physical society*. (Vol. 68, pp. 493–503). IOP Publishing. <https://doi.org/10.1088/0370-1301/68/8/302>
- Takahashi, H., Costa, S., Otsuka, Y., Shiokawa, K., Monico, J. F. G., Paula, E., et al. (2014). Diagnostics of equatorial and low latitude ionosphere by TEC mapping over Brazil. *Advances in Space Research*, *54*(3), 385–394. <https://doi.org/10.1016/j.asr.2014.01.032>
- Takahashi, H., Wrasse, C. M., Denardini, C. M., Pádua, M. B., de Paula, E. R., Costa, S. M. A., et al. (2016). Ionospheric TEC weather map over South America. *Space Weather*, *14*(11), 937–949. <https://doi.org/10.1002/2016SW001474>
- Takahashi, H., Wrasse, C. M., Otsuka, Y., Ivo, A., Gomes, V., Paulino, I., et al. (2015). Plasma bubble monitoring by TEC map and 630 nm airglow image. *Journal of Atmospheric and Solar-Terrestrial Physics*, *130*, 151–158. <https://doi.org/10.1016/j.jastp.2015.06.003>
- Wanninger, L. (1993). The occurrence of ionospheric disturbances above Japan and their effects on precise GPS positioning. *Proceedings of the CRCM*, *93*, 6–11.
- Wrasse, C. M., Nakamura, T., Tsuda, T., Takahashi, H., Medeiros, A. F., Taylor, M. J., et al. (2006). Reverse ray tracing of the mesospheric gravity waves observed at 23 S (Brazil) and 7 S (Indonesia) in airglow imagers. *Journal of Atmospheric and Solar-Terrestrial Physics*, *68*(2), 163–181. <https://doi.org/10.1016/j.jastp.2005.10.012>